International Journal of Fluid Power 14 (2013) No. 2 pp. 17-26

AN ANALYTIC THERMODYNAMIC MODEL FOR HYDRAULIC RESISTANCES BASED ON CFD FLOW PARAMETERS

Christian von Grabe, Christian Riedel, Christian Stammen and Hubertus Murrenhoff

RWTH Aachen University, Institute for Fluid Power Drives and Controls (IFAS), Steinbachstr. 53, 52074 Aachen, Germany
Christian.vonGrabe@ifas.rwth-aachen.de, Christian.Riedel@ifas.rwth-aachen.de,
Christian.Stammen@ifas.rwth-aachen.de, mh@ifas.rwth-aachen.de

Abstract

This article illustrates the development of an analytic lumped parameter thermo-hydraulic model for a wide range of hydraulic resistance geometries based on mass flow. The relevant flow parameters such as the contraction coefficient in case of laminar flow separation are derived from CFD simulations. Furthermore, the consideration of cavitation effects can be included.

State of the art in lumped parameter simulations of hydraulic circuits utilise volume-flow based equations like the orifice equation, which is extended for a wide variety of geometries and flow conditions including the transition from laminar to turbulent flow by adjusting the discharge coefficient based on empirical equations or lookup tables. The same situation persists for laminar flow description. In this case the Hagen-Poiseuille equation is often used in conjunction with correction factors based on the Reynolds number to regard the transition of laminar to turbulent flow. However, in practical applications the use of different equations for various flow conditions and geometries is cumbersome. Furthermore, in the widely used volume based flow description, the absolute pressure dependency of mass flow due to density changes and critical flow at which cavitation occurs is not accounted for until now. Without consideration of these influences a mass conservative modelling and thus high model precision is not possible. The overall goal of the proposed model is to increase accuracy of hydraulic system simulation tools and to support usability by simplifying parameterisation on basis of dimensions available from data sheets. The results of this study are obtained analytically as well as empirically by means of CFD simulations. Moreover, a large number of performed simulations support the understanding of fundamental effects in hydraulic resistance flow.

Keywords: lumped parameter, thermo-hydraulic simulation, hydraulic resistance, orifice, throttle, CFD, cavitation

1 Introduction

1.1 Mass Flow Based System Simulation

Lumped parameter system simulation tools are state of the art in research and development of fluid power systems. Validity of the simulated behaviour is greatly influenced by the level of detail and parameterisation of the models. The accuracy of simulation results depends on the quality of the basic models that represent the physical effects (Watton, 2007). The central components of lumped parameter simulations are the hydraulic capacity, inductivity and resistance. In the fundamentals of fluid power these basic components are conventionally modelled based on a volume conservative approach. The conservation of mass is reduced to conservation of volume in most hydraulic simulation tools. This is not a valid simplification for all cases. The constant density volume flow does not match the real flow without additional corrections. In closed systems with many pressure changes over time small deviations add up to significant errors in calculation of the system behaviour. However, only a consistent use of mass flows and volume changes exactly complies with the equation of continuity as shown by Riedel et al. (2010).

In such an isothermal lumped parameter system simulation the mass flow $\dot{m}$ through the component is calculated as a function of pressure difference Δp between the components. The pressure build-up is calculated in the mass nodes as a function of bulk modu-

This manuscript was received on 02 July 2012 and was accepted after revision for publication on 20 March 2013

lus E, mass flows $\dot{m}$ and volume change $\dot{V}$ (Nykänen et al., 2000; Riedel et al., 2009). In a thermo-hydraulic simulation the heat flow $\dot{W}$ is calculated as a function of heat capacity c_p, density ρ and pressure difference Δp (Baum, 2001). However, in many cases the conventional volume flow approach is chosen even for a thermo-hydraulic simulation, thus the mass and hence the energy balance is not exact.

The thermo-hydraulic simulation has great potential due to the strong temperature dependency of fluid parameters, as shown by Witt (1974), although heat convection requires a very complex and difficult parameterisation.

Besides capacities and inductivities derived for the mass conservative case by Riedel et al. (2009), hydraulic resistances of any given degree of complexity are a central component of lumped parameter modelling, but pose the greatest challenge due to complex flow behaviour through real geometries. Therefore the authors suggest an advanced thermodynamic resistance model, which is parameterised from geometric values and besides by a contraction coefficient derived from CFD simulations.

1.2 Hydraulic Resistances

Technical resistances in hydraulics are conventionally modelled either as throttles (*laminar flow*) or orifices (*turbulent flow*) as described by Murrenhoff (2007).

Orifice:

The following Eq. 1 applies for mass flow through an orifice based on the incompressible Bernoulli equation at steady state:

$$\dot{m} = \pi \cdot r^2 \cdot \alpha_D \cdot \sqrt{2 \cdot \Delta p \cdot \rho} \tag{1}$$

The discharge coefficient α_D of hydraulic resistances comprises all losses due to friction. It strongly depends on inlet geometry and ratio between length l and inner diameter d according to Fig. 3, which also affect the contraction coefficient α_K.

Furthermore, the Reynolds number Re, as a function of flow velocity u, hydraulic diameter d_h and kinematic viscosity ν, has a great influence on the discharge coefficient α_D (Murrenhoff, 2007). At low Re-values (laminar) a steady increase can be observed, whereas the coefficient shows almost constant behaviour in the turbulent region. A transient area can be observed in between (Latour, 1996; Eich, 1979). Overall, the following Eq. 2 is applicable for the discharge coefficient α_D of a resistance shown in Fig. 3:

$$\alpha_D = f\left(A_1, A_k, u_k, \rho, \eta\right) \tag{2}$$

Measurements of resistance geometries by Riedel (1973), Beater (1999) and Idelchik (2007) show that the discharge coefficient strongly depends on the degree of turbulence. In the laminar area the coefficient is proportional to the square root of the Reynolds number Re, whereas at higher Re-values it stays constant. The transient area between laminar and turbulent flow may be marked as the critical Reynolds number Re_{crit}. According to Beater this value can be found between 100 and 200 for orifices. The following Fig. 1 shows an exemplary flow with $\alpha_{Dmax} \approx 0.64$.

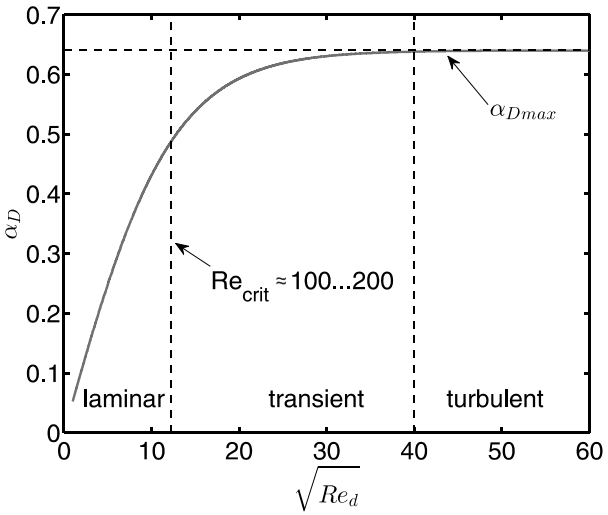

Fig. 1: *Dependency of discharge coefficient α_D on Reynolds number Re (Beater, 1999)*

Throttle:

The mass conservative flow through a throttle can be described as follows based on the Hagen-Poiseuille law with an incompressible fluid at steady state:

$$\dot{m} = \frac{\pi \cdot r^4}{8 \cdot \nu \cdot l} \cdot \Delta p \tag{3}$$

The following Fig. 2 illustrates the significant temperature influence on the discharge through a throttle with fluid parameters of a HLP 46 oil irrespective of choking conditions due to cavitation and friction. For reasons of accuracy the inner change of the state variable was numerically integrated over the length of the throttle.

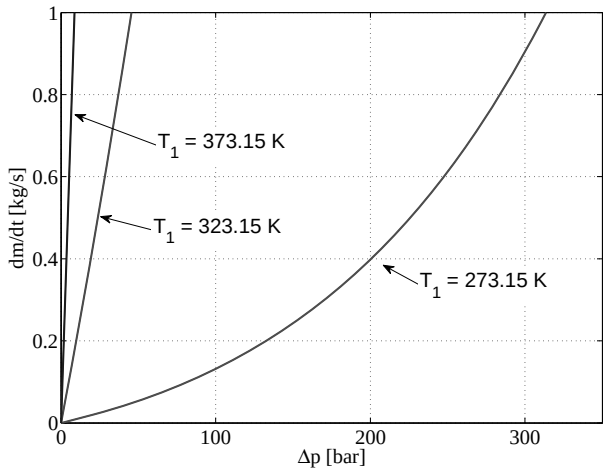

Fig. 2: *Temperature influence on throttle*

However, these simple resistances only apply for certain components. Any other transient form may only be accounted for completely empirically so far (see Idelchik, 2007).

Other components, such as valves, show a more complex flow pattern that strongly depends on the spool position. Among others, Maré et al (2008) have

conducted research on one-dimensional modelling of proportional valves. The discharge coefficient α_D can be described as a function of the Reynolds number *Re* and the spool position.

Figure 3 depicts the scheme of a more complex hydraulic resistance, which can neither be matched to a pure orifice nor pure throttle. As most of real resistances found in hydraulic systems the depicted resistance is a combination of both. In addition, the figure illustrates the static pressure along the geometry at inlet (1), contraction region (k), expansion (2) and outlet (3).

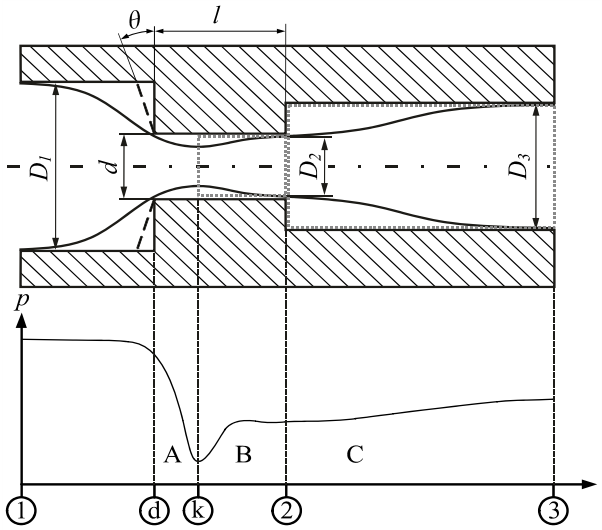

Fig. 3: *Scheme of hydraulic resistance and static pressure*

Besides experimental work there are empirical models of flow parameters, which, however, have many restrictions. In case of an orifice the *Reader-Harris/Gallagher* equation applies, which is used in the *DIN EN ISO 5167-2* (2004). Another description was proposed by Merrit (1967), which depends on the Reynolds number *Re* and the geometry.

Luhmer (1981) uses laminar factors to describe an increasing *l*/*d* ratio up to 1.67. The parameters *K* and *z* in Eq. 4 were determined empirically and are available in lookup tables for different geometric parameters as well as laminar and turbulent flow (Luhmer, 1981; Beater, 1999).

$$Q = K \cdot \Delta p^z \tag{4}$$

Idelchik (2007) makes use of the resistance coefficient ξ in Bernoulli's equation to determine pressure difference based on density ρ and inlet velocity u_1.

$$\Delta p = \xi \cdot \frac{\rho \cdot u_1^2}{2} \tag{5}$$

The resistance coefficient ξ may be calculated by means of the empiric Eq. 6 in case of an orifice ($D_1 = D_2$, $l/d < 0{,}015$ and $Re > 10^5$) as follows (Idelchik, 2007).

$$\xi = \frac{2\Delta p}{\rho u_d^2} = \left[\left(1 - \frac{A_d}{A_1}\right) + 0{,}707 \left(1 - \frac{A_d}{A_1}\right)^{0{,}375} \right]^2 \left(\frac{A_1}{A_d}\right) \tag{6}$$

Besides α_D and ξ the flow contraction α_K is a relevant parameter for the characterization of hydraulic resistances, which is dependent on geometry and directly correlates with the pressure drop Δp_v. The following Carnot equation describes how much impulse is lost in the flow due to friction (Schröder, 2004) and thus describes idealized conditions for the anticipated minimal pressure loss in an orifice ($l = 0$).

$$\Delta p_v = \frac{\rho}{2} u_k^2 \left[1 - \left(\frac{A_k}{A_3} \right) \right]^2 \tag{7}$$

Together with the continuity equation and the cross section ratio A_d / A_1 as well as the contraction coefficient $\alpha_K = A_k / A_d$ we receive a description for the pressure difference depending on inlet velocity u_1 and the ratios A_d/A_1 and α_K.

$$\Delta p_v = \frac{\rho}{2} u_1^2 \left[\frac{1 - \alpha_K \cdot A_d / A_1}{\alpha_K \cdot A_d / A_1} \right]^2 \tag{8}$$

Figure 4 depicts the pressure Δp_v depending on the cross sectional ratios with density $\rho = 880\ kg/m^3$ (incompressible fluid) and inlet velocity $u_1 = 4\ m/s$ based on the Carnot equation. Obviously the ratio A_d/A_1 has a large influence on the pressure drop, whereas a change of flow contraction α_K leads to significant losses only at higher values.

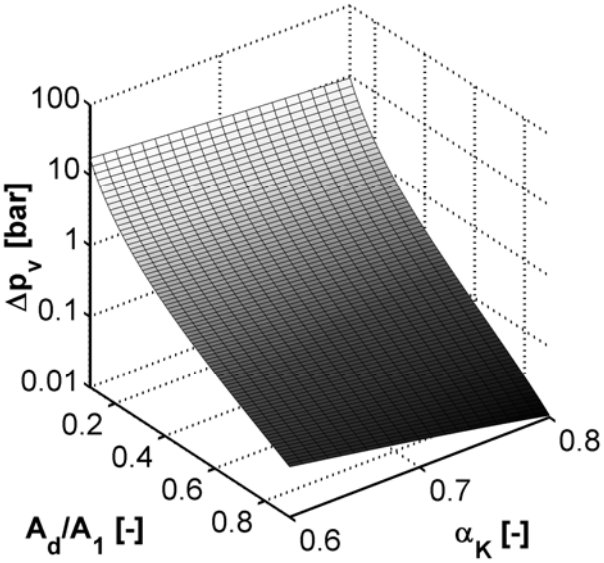

Fig. 4: *Pressure loss Δp_v in dependency of cross sectional ratios within orifice geometry*

1.3 Fluid Parameters

The density ρ and dynamic viscosity η are the most important fluid properties in simulation of hydraulic resistances and are functions of temperature *T* and pressure *p* as shown by Witt (1974). Among others alternative fluid data is available from the SAE information report 1362 (SAE, 2000). State of the art simulation tools consider these nonlinear dependencies. In thermo-hydraulic simulations, the fluid's heat capacity c_p is incorporated as well in order to calculate the heat flow $\dot{W}$ (Baum**,** 2001). However, for advanced thermodynamic modelling the derived parameters specific enthalpy *s*, entropy *h* and inner energy *e* must be ac-

counted for as well (Witt, 1974). In this study the models by Witt were chosen due to high accuracy as well as availability of derived thermodynamic parameters (Baum**,** 2001). To provide the same boundary conditions for the simulation model and the CFD-simulation, the Witt-equations (Witt 1974) were implemented in the CFD fluid model as well as the resistance model introduced in the following paragraph.

2 Resistance Model

2.1 Non-Cavitating Flow

The goal of this research is an accurate analytic description of flow through hydraulic resistances. The scheme in Fig. 3 illustrates that the flow may be divided into three characteristic sections. The first section A starts at the inlet 1 and ends at the point of maximal contraction of the streamlines k. At this point the lowest static pressure can be observed. The second section is situated in between k and the end of contraction 2. The third section C ends at the outlet 3 of the resistance. As flow is decelerated due to expansion subsequently, static pressure increases again.

In the first case only non-cavitating flow should be considered. Based on the equation of continuity mass is conserved within a resistance as follows with a mean velocity u:

$$\begin{aligned}\dot{m} &= A_1 \cdot \rho_1 \cdot u_1 = A_\mathrm{k} \cdot \rho_\mathrm{k} \cdot u_\mathrm{k} \\ &= A_2 \cdot \rho_2 \cdot u_2 = A_3 \cdot \rho_3 \cdot u_3\end{aligned} \tag{9}$$

The energy balance is taken into account for the description of the change of state in the first section (1 → k). The first law of thermodynamics states:

$$q_{1\mathrm{k}} + w_{1\mathrm{k}} = h_\mathrm{k} - h_1 + \frac{1}{2}\left(u_\mathrm{k}^2 - u_1^2\right) + g\left(z_\mathrm{k} - z_1\right) \tag{10}$$

The change of geodetic height within the resistance may be neglected. It may only be important for long pipe-like resistances in vertical position. In case of an adiabatic and steady flow in the first section we receive:

$$\begin{aligned}h_1 + \frac{1}{2}u_1^2 &= h_\mathrm{k} + \frac{1}{2}u_\mathrm{k}^2 \\ e_1 + \frac{p_1}{\rho_1} + \frac{1}{2}u_1^2 &= e_\mathrm{k} + \frac{p_\mathrm{k}}{\rho_\mathrm{k}} + \frac{1}{2}u_\mathrm{k}^2\end{aligned} \tag{11}$$

Substitution of velocities u by the equation of continuity leads to the mass flow shown in Eq. 12:

$$\dot{m} = \sqrt{2\frac{\left(\frac{p_1}{\rho_1} - \frac{p_\mathrm{k}}{\rho_\mathrm{k}}\right) + \left(e_1 - e_\mathrm{k}\right)}{\frac{1}{A_\mathrm{k}^2 \rho_\mathrm{k}^2} - \frac{1}{A_1^2 \rho_1^2}}} \tag{12}$$

Additionally, external heat fluxes may be incorporated into the respective sections. For a parameterisation only external variables are available in most cases. The model must be able to describe the state variables within the component in dependency of accessible parameters. Losses due to friction, stream expansion and eddies in the post contraction zone are included by means of conservation of momentum. The dotted line in Fig. 3 depicts the corresponding balancing area and is chosen in analogy to a step diffuser (Jungemann, 2005; Truckenbrodt, 1996; Schröder, 2004).

For small length to diameter ratios $l/d < 0{,}5$ the friction losses at the wall may be neglected (Riedel, 1973). If the ratio is increasing a friction model, as described by Beater (1999), is used. The wall friction is calculated based on the grade of turbulence represented by the Reynolds number Re.

Considering the pressure loss at the wall Δp_Wall we receive the following Eq. 13 for the second section (k → 2):

$$\dot{m}\left(u_\mathrm{k} - u_2\right) = \left(p_2 - p_\mathrm{k} + \Delta p_\mathrm{Wall}\right) A_\mathrm{d} \tag{13}$$

The third section (2 → 3) may be modelled without wall friction as the diameter increases and thus, flow velocity is sufficiently small. Furthermore, inlet and outlet length of a component are relatively short. With this assumption we receive:

$$\dot{m}\left(u_2 - u_3\right) = \left(p_3 - p_2\right) A_3 \tag{14}$$

However, in some components, such as valves, this might become a relevant issue at higher flow rates.

Substituting velocities u by Eq. 9, transforming Eq. 13 to p_k and Eq. 14 to p_2 results into a description of pressure p_k in the contraction area, which is only dependent on known parameters, except for the contraction area A_k. Based on the pressure p_k, representing the lowest pressure (in case the wall friction is smaller than pressure regeneration effects), cavitating flow can be evaluated. The ratio between A_k and A_2 is described by the contraction coefficient α_k, which will be determined by means of CFD simulations in the following chapter.

$$\begin{aligned}p_\mathrm{k} = p_3 + \Delta p_\mathrm{Wall} &+ \frac{\dot{m}^2}{A_3}\left(\frac{1}{\rho_3 A_3} - \frac{1}{\rho_2 A_2}\right) \\ &+ \frac{\dot{m}^2}{A_\mathrm{d}}\left(\frac{1}{\rho_2 A_2} - \frac{1}{\rho_\mathrm{k} A_\mathrm{k}}\right)\end{aligned} \tag{15}$$

Combining Eq. 12 and 15 yields the mass flow as a function of p_1 and p_3:

$$\begin{aligned}\dot{m} &= \sqrt{\frac{X}{Y+Z}} \\ X &= 2\left(\left(\frac{p_1}{\rho_1} - \frac{p_3 + \Delta p_\mathrm{Wall}}{\rho_\mathrm{k}}\right) + \left(e_1 - e_\mathrm{k}\right)\right) \\ Y &= \frac{1}{A_\mathrm{k}^2 \rho_\mathrm{k}^2} - \frac{1}{A_1^2 \rho_1^2} \\ Z &= \frac{2}{A_3 \rho_\mathrm{k}}\left(\frac{1}{\rho_3 A_3} - \frac{1}{\rho_2 A_2}\right) + \\ &\quad \frac{2}{A_\mathrm{d} \rho_\mathrm{k}}\left(\frac{1}{\rho_2 A_2} - \frac{1}{\rho_\mathrm{k} A_\mathrm{k}}\right)\end{aligned} \tag{16}$$

Besides pressure, fluid parameters such as density ρ and inner energy e are input variables which are available from mentioned fluid models. Calculation of den-

sity and energy requires temperature and pressure values at the given locations.

Assuming an isentropic condition $s_1(p_1,T_1) = s_k(p_k,T_k)$ is valid in this section and T_k may be calculated. T_k may be solved numerically only due to the complexity of the entropy fluid model. Together with known p_k all other relevant parameters may be determined.

Concerning temperatures at point 2 and 3 we revert to the first law of thermodynamics, which yields the change of state between 1 and 2:

$$e_1 + \frac{p_1}{\rho_1} + \frac{1}{2}\left(\frac{\dot{m}}{\rho_1 A_1}\right)^2 = e_2 + \frac{p_2}{\rho_2} + \frac{1}{2}\left(\frac{\dot{m}}{\rho_2 A_2}\right)^2 \quad (17)$$

Respectively between 1 and 3 it states:

$$e_1 + \frac{p_1}{\rho_1} + \frac{1}{2}\left(\frac{\dot{m}}{\rho_1 A_1}\right)^2 = e_3 + \frac{p_3}{\rho_3} + \frac{1}{2}\left(\frac{\dot{m}}{\rho_3 A_3}\right)^2 \quad (18)$$

It becomes apparent that Eq. 17 and 18 may only be solved numerically as well because inner energy e respectively depends on temperature in the corresponding sections.

If an ideal orifice must be described, Eq. 16 simplifies as only two sections remain due to the minimal length to diameter ratio l/d. Without pressure loss as a result of viscous friction inside the resistance, the orifice flow is virtually independent of fluid viscosity. Furthermore, the wall friction term can be omitted. In analogy to the throttle model the law of momentum can be applied to the second section. Therefore, the orifice mass flow resolves into:

$$\dot{m} = \sqrt{\frac{2\left(\left(\frac{p_1}{\rho_1} - \frac{p_2}{\rho_k}\right) + \left(e_1 - e_k\right)\right)}{\frac{1}{A_k^2 \rho_k^2} - \frac{1}{A_1^2 \rho_1^2} + \frac{2}{A_2 \rho_k}\left(\frac{1}{\rho_2 A_2} - \frac{1}{\rho_k A_k}\right)}} \quad (19)$$

The pressure at the outlet of the orifice is known so that temperature T_2 may be calculated numerically in analogy to the throttle model based on the first law of thermodynamics and the fluid model.

2.3 Cavitating Flow

In case of cavitating flow through a resistance the mass flow may not be increased any further. Cavitation occurs when static pressure drops within the flow field to a critical value. In a throttle the highest velocity and thus the lowest static pressure occurs at the contraction point k, where local cavitation areas build up. However, actual blocking of mass flow occurs when pressure within the core flow drops down to the fluid's vapour pressure p_v and thus spreads across the whole cross section (Schmitt, 1966).

Further pressure reduction is hindered due to increased vaporisation (Schmitt, 1966; Riedel, 1973; Jungemann, 2005).

For this reason pressure calculation according to Eq. 15 becomes obsolete. Instead pressure p_k may be replaced by vapour pressure p_v. Density ρ_v is chosen for the fluid phase at vapour pressure. Based on these simplifications we obtain the mass flow in cavitating state:

$$\dot{m}_{\text{cavitation}} = \sqrt{\frac{2\left(\left(\frac{p_1}{\rho_1} - \frac{p_V}{\rho_V}\right) + \left(e_1 - e_k\right)\right)}{\frac{1}{A_k^2 \rho_v^2} - \frac{1}{A_1^2 \rho_1^2}}} \quad (20)$$

According to Eq. 20 no conclusions can be drawn from state variables downstream of the cavitation area or transient area between non-cavitating and cavitating flow. This information could be made available by an model based description of cavitating flow starting in k to describe the flow conditions downstream.

Furthermore, any occurring hysteresis effects described by Riedel (1973) cannot be modelled this way.

A cavitating orifice may be modelled based on the same methodology with Eq. 19 as a basis.

The mass flow equation of an orifice and throttle are the same in case of cavitating flow, because only the first section from $1 \rightarrow k$ is necessarily regarded. For greater lengths of a throttle the wall friction becomes relevant again. However, Riedel (1973) shows that in case of orifices at beginning of cavitation an unsteady volume flow occurs. It is not clear, if this behaviour is caused by a change of state, e.g. vapour pressure p_V or density ρ or a change of the flow contraction α_K.

Riedel reflects that the unsteady behaviour is caused by an unsteady change of flow. If the phenomenon is caused solely by a change of flow contraction and thus A_k, the proposed Eq. 20 remains valid. An accurate CFD simulation of a cavitating flow is not possible so far, as parameters for the Rayleigh-Plesset equation are not available for hydraulic oils at this point (Yang et al, 2005). Therefore, the validity of the proposed cavitation model cannot be analysed in course of this study and is subject to future work.

3 CFD-Based Analysis of Resistances

Besides geometric and fluid parameters the proposed analytic model for hydraulic resistances must be parameterised by the contraction coefficient α_K, which cannot easily be measured in test stand trials. Conventionally this parameter is determined in free flow tests, which lack in accuracy due to missing counter pressure effects. Therefore, the authors suggest a CFD-based methodology that grants access to the inner flow behaviour. Moreover, it allows for a detailed analysis of parameter correlations and interdependencies in course of a statistical analysis, which has only been possible in prior experimental studies to a limited extend (Riedel, 1976; Idelchick, 2007). Another way to determine the contraction coefficient α_K would be by measurement in analogy to the discharge coefficient α_D. The disadvantage of using experimentally determined characteristics is the absence of any physical motivation because the results could be adjusted by altering α_K to match measured results, even if α_K is only one influence among many that alter the mass flow. The au-

thor's approach focuses on separation of theflow contraction effect and others such as wall friction.

For this purpose non-isothermal models are simulated in ANSYS CFX with the SST turbulence model. Additionally, pressure and temperature dependent fluid parameters were implemented according to Witt (1974). Based on the Grid-Convergence Index (GCI) defined by Roach (1997) a design study was performed in order to find a balance between discretisation error due to mesh size and resulting simulation time. Approximately 300.000 elements were chosen for a 30° rotational segment shown in Fig. 5 that shows no change in the simulation results compared to meshes with 500 k, 900 k and 2 mio. elements.

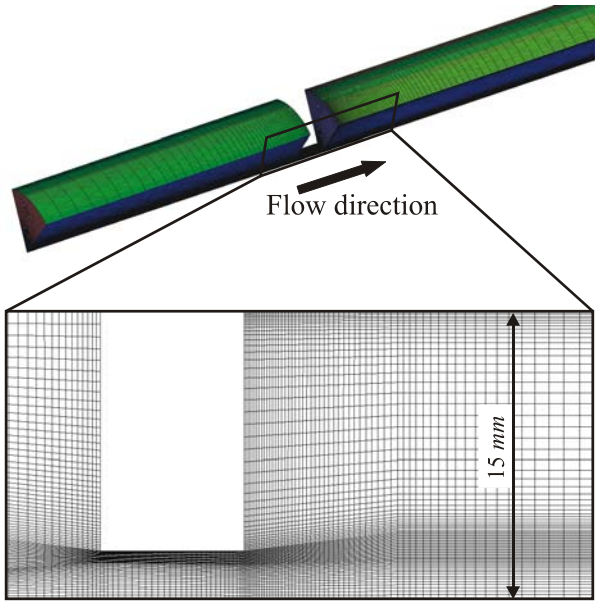

Fig. 5: *Mesh structure of 30° rotational segment*

In a primary CFD study relevant parameters, which significantly influence the flow behaviour and thus contraction α_K, have been identified for further analysis. Both physical parameters mass flow $\dot{m}$ and temperature T_1 as well as geometric parameters inlet angle θ, diameter d_2 and length l are varied according to a carefully chosen experimental plan in order to keep simulation time as low as possible. As most influences and output parameters are second order functions, it is sufficient in most cases to choose a variation of three to five points per parameter. Based on fundamentals of fluid mechanics and empirical analyses of the past, it is known that not all parameters show a high degree of interaction (Murrenhoff, 2007; Latour, 1996; Eich, 1979). A comparison of CFD simulations with measurements by Riedel (1973) for different geometries and own measurements demonstrates the validity of the models. The following Table 1 illustrates exemplary results of discharge coefficient α_D for different l/d ratios and the error of $\alpha_{D,\,CFD}$ referred to measured $\alpha_{D,\,Meas}$:

Table 1: Comparison of discharge coefficient α_D between CFD simulations and measurements (Lichtarowicz, 1965)

d [mm]	l/d ratio [-]	$\alpha_{D,\,CFD}$ [-]	$\alpha_{D,\,Meas.}$ [-]	*Error* [%]
3	0	0,627	0,62	1,13
3	1,25	0,737	0,77	4,29
3	2,5	0,779	0,81	3,83
3	5	0,786	0,79	0,51
5	0	0,625	0,62	0,81
5	0,75	0,703	0,72	2,36
5	1,5	0,776	0,79	1,77
5	3	0,803	0,80	0,38
7	0	0,633	0,62	2,10
7	0,54	0,690	0,68	1,47
7	1,07	0,769	0,76	1,18
7	2,14	0,817	0,81	0,86

The following Fig. 6 shows the high accuracy of CFD and lumped parameter models in comparison with measurements, orifice and throttle equations for an exemplary resistance (dimensions depicted) at 25 °C as well as 40 °C. Furthermore, the results of an empirical model by Idelchik (2007, p. 379) are depicted. The influence of the inlet angle θ is neglected, because no adequate formulation is provided. A comparison with Luhmer (1981) is abandoned due to the restriction of l/d ratios up to 1,67.

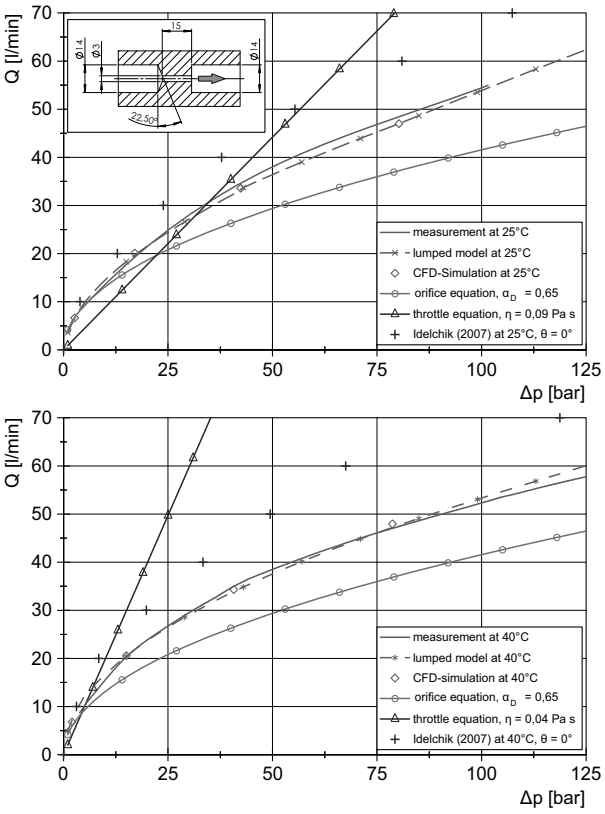

Fig. 6: *Comparison of measurements, CFD-simulations, orifice, throttle and lumped parameter model*

In order to define the flow contraction α_K a streamline is placed in CFD as close to the inlet edge. It must be pointed out that the total course of the streamline within the component is relevant as a second contraction area at the outlet of a throttle has to be taken into account for the law of momentum, if flow has not attached to the wall yet. Another streamline is set on the rotational axis to determine the minimal pressure p_{min}, temperature T_{min} and velocity u_{max}. These values might not be located at the highest flow contraction, but further downstream due to the flow pattern.

3.1 Influence of Length *l*

The ratio *l*/*d* is highly relevant for the flow behaviour (Riedel, 1973; Lichtarowicz, 1965). Starting at a pure orifice, which is solely dependent on fluid density ρ, the pressure drop decreases with increasing length. At a ratio $l/d \approx 2$ the pressure drop reaches its minimum and then increases due to viscous friction. Pressure regain effects are responsible for the nonlinear behaviour, as the flow attaches to the walls again after contraction and thus leads to a better guiding. As viscous friction comes into account, being directly correlated to dynamic viscosity η, temperature influence rises with length. However, temperature influence on pressure loss is highly dependent on $\dot{m}$ and thus *Re*. At low *Re* values the influence is significant while it becomes obsolete at higher turbulence, because friction losses are lower in case of a turbulent flow in comparison to a laminar flow for smooth surfaces, when neglecting differences in mean flow velocity *u* and density ρ. The following Fig. 7 depicts Δp over *l*/*d* for different temperatures at a low mass flow $\dot{m}$ of 0.7 kg/s.

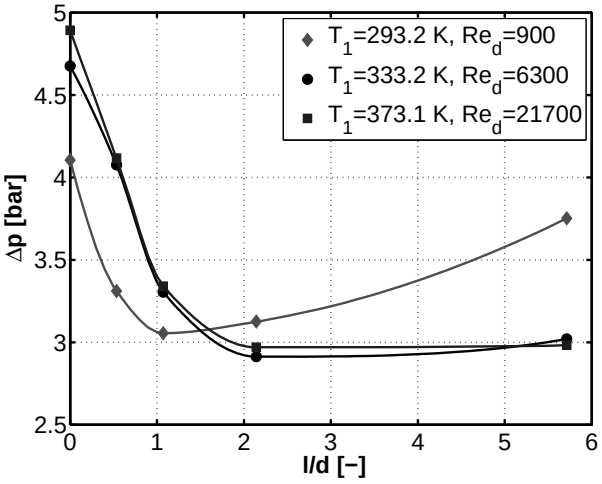

Fig. 7: *Pressure losses Δp over ratio l/d at constant mass flow 0,7 kg/s for d = 7 mm and D = 30 mm*

3.2 Influence of inlet angle θ

While the influence of the ratio *l*/*d* on discharge is documented quite well in literature, the inlet angle θ has not gained much attention. It is assumable that the flow contraction is mostly influenced by the mass forces within the fluid. Therefore, the inlet angle should strongly correlate with the contraction and thus pressure loss, as change in flow direction decreases.

The following Fig. 8 shows the influence of the inlet angle on the pressure difference. As mass flow rises the relative temperature influence becomes obsolete. At angles θ above 35° the slope of the pressure loss increases due to the change of an impact flow to guided flow. At a low flow rate the relative influence of temperature is significant, as flow attached earlier to the wall again which increases friction losses on the other hand.

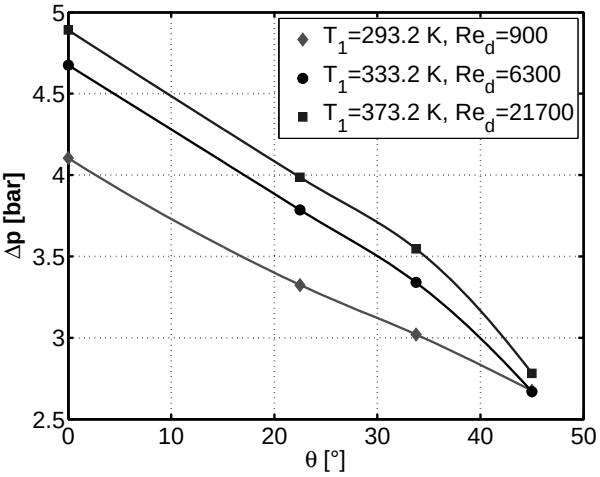

Fig. 8: *Pressure losses Δp over inlet angle θ at constant mass flow 0,7 kg/s for d = 7 mm and D = 30 mm*

The following Fig. 9 shows the pressure loss over the two discussed geometric parameters *l*/*d* ratio and inlet angle θ at a constant temperature $T_1 = 333{,}15$ K and a diameter $d = 7$ mm and clearly depicts the interdependencies. With increasing *l*/*d* ratio the pressure loss and influence of angle θ drop significantly. The better the flow guiding the higher is α_K, which means that within the throttle flow attaches again at an earlier stage. This indicates that friction losses overcompensate pressure regain effects at even lower *l*/*d* ratios.

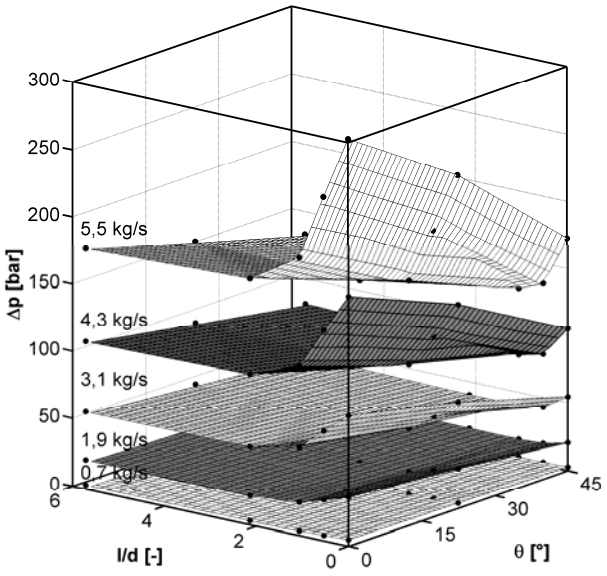

Fig. 9: *Pressure loss over l/d ratio and inlet angle θ for different mass flow rates at temperature $T_1 = 333{,}15$ K and diameter d = 7 mm*

The central element of the CFD-based research is the contraction coefficient representing a great share of the overall pressure losses within the component. Figure 10 depicts α_K over l/d and θ. It becomes obvious that the mass flow influence is relatively small compared to geometric parameters. However, at low flow rates it differs slightly due to laminar friction and intersects with the values at higher flow rates due to the fact that α_K increases again in the laminar region with decreasing *Re*-values (Will, 1968). Consequently α_K shows a dependency on Re in the laminar and transition region, which increases with l/d ratios due to wall friction effects. At turbulent flow this effect relieves and leads to independency of α_K from flow rate.

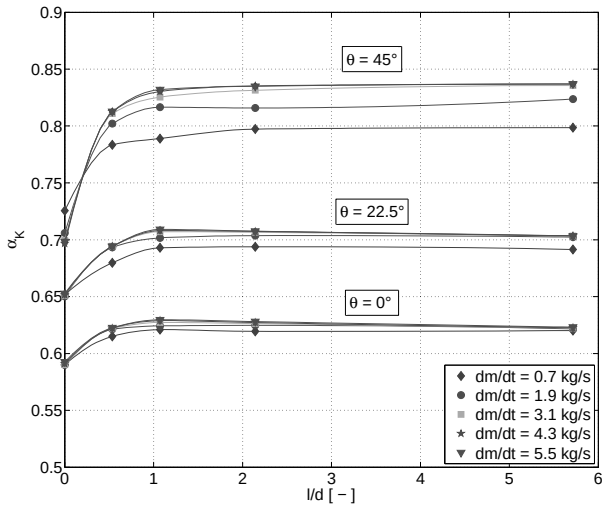

Fig. 10: *Contraction coefficient α_K over l/d ratio and inlet angle θ for different mass flow rates at temperature T_1 = 333,15 K and diameter d = 7 mm*

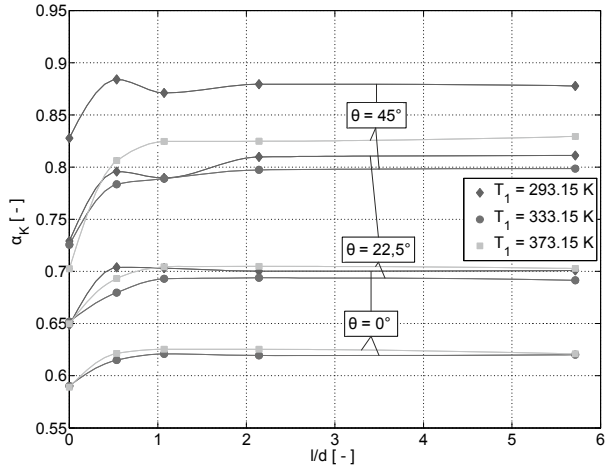

Fig. 11: *Contraction coefficient α_K over l/d ratio and inlet angle θ for different temperatures at mass flow $\dot{m}$ = 0.7 kg/s and diameter d = 7 mm*

Whereas influence of mass flow is low, the contraction coefficient α_K significantly changes with temperature, as shown in Fig. 11. Low viscosity at high temperatures results in increased contraction and decreased coefficient. However, this influence decreases as mass flow rises and flow becomes more turbulent. At low l/d ratios there is a small peak of the coefficient visible. Pressure regain effects, shown in Fig. 5, are responsible for these phenomena and are responsible for the pressure minima at this point.

3.3 Analysis of Lumped Model

When we revert to the determined α_K values and the fluid model by Witt (1974) and compare these values with the CFD simulations we may analyse the deviations and thus the quality of the proposed model. However, it must be made clear that the determination process of α_K from the CFD simulations might already include inaccuracies due to the chosen approach with streamlines. Main deviations can be observed in the laminar regions, at which α_K is very high due to low flow rate. At higher l/d ratios the flow can attach to the walls again which leads to friction that must be accounted for. Although the introduced friction model leads to better results than neglecting friction, deviations remain. At this point it is not clear, if the chosen friction model or the simulation properties are responsible. The following Fig. 12 shows deviations between the proposed lumped model and CFD over l/d ratio and inlet angle θ. Combining all deviations to the CFD simulation for the analyzed cases we receive a mean value of 4,2 % for all geometries based on the mass flow. Figure 12 illustrates the relative deviation of mass flow $\dot{m}$. The shown values represent the mean absolute error for each geometry case. Thus, each point represents a multitude of different *Re*-values. Only in certain cases the deviation amounts to more than 5 %. At $\theta = 45°$ the contraction decreases significantly which results into difficulties in the extraction of the values from CFD simulations. The largest diameter results into the highest deviations.

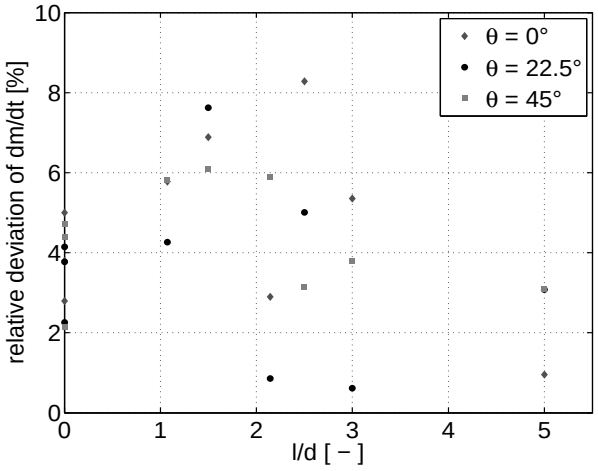

Fig. 12: *Relative mass flow deviations between lumped parameter model and CFD simulation*

4 Summary and Outlook

Widely used volume flow based hydraulic resistance models lack the ability to describe the absolute pressure dependency of mass flow due to density changes and critical flow at which cavitation occurs exactly. Further model deviations are induced due to the simplification of

constant fluid parameters within the component. As the occurrence of cavitation at hydraulic resistances is a major problem in many applications, a model is highly desirable, which allows for detection of possible cavitation effects and assessment of further flow behaviour during cavitating state.

However, even for complex simulation models, the general objective must be a parameterisation based only on accessible geometric and physical parameters, such as inlet and outlet pressures and inlet temperature.

The proposed analytical model for hydraulic resistances comprises the above mentioned features under the set boundary conditions. Although the model is of analytic nature to a large extent, few empiric values persist. In any case the thermodynamic fluid properties must be described by means of empiric models. In course of this research the models proposed by Witt (1976) were chosen for HLP 46 oil which are available for many other fluids as well.

The remaining flow parameter in the model is the contraction coefficient α_K, which is very difficult to measure in test stand trials. However, this parameter is determined based on CFD simulations for a multitude of geometries and flow conditions. As anticipated, the simulations show a great dependency on geometric parameters. Resulting, we may revert to either a lookup-table or a mathematical description for α_K, which serves as input for the resistance model. Results of CFD simulations were compared to measurements in order to validate the accuracy. Altogether we receive a highly accurate model for a large variety of hydraulic resistances. The overall mean deviations without any further adaption to the CFD simulation for the analysed cases are 2,4 % for an orifice and 4,9 % for a throttle geometry. Deviations occur mainly at laminar flow due to possible inaccuracies in determination of α_K and in case of large l/d ratios due to wall friction.

In case of a cavitating flow a possibility for modelling has been proposed based on observations among others by Jungemann (2005) and Riedel (1976). An extended evaluation of model validity remains difficult, as cavitation is influenced by a large number of factors not being considered in the model. Further analysis of such properties is subject to future work.

Acknowledgement

We would like to thank the German Research Foundation (DFG) for funding the project “Mass Conservative System Simulation”.

Nomenclature

A	Cross section area	[m^2]
c_p	Specific heat capacity	[J/kg/K]
d	Inner Diameter	[m]
D	Outer Diameter	[m]
e	Specific inner energy	[J/kg]
E	Bulk modulus	[bar]
h	Specific enthalpy	[J/kg]
l	Length	[m]
k	Flow contraction	[-]
K	Laminar factor	[-]
m	Mass	[kg]
p	Absolute pressure	[bar]
r	Radius	[m]
s	Specific entropy	[J/kg/K]
T	Temperature	[K]
u	Velocity	[m/s]
V	Volume	[m^3]
$\dot{w}$	Heat flow	[J/s]
z	Laminar factor	[-]
α_D	Discharge coefficient	[-]
α_K	Contraction coefficient	[-]
η	Dynamic viscosity	[kg/m/s]
θ	Inlet angle	[°]
ν	Kinematic viscosity	[m^2/s]
ξ	Resistance coefficient	[-]
ρ	Density	[kg/m^3]

References

Avva, R. K., **Singhal, A.** and **Gibson, D. H.** 1995. An Enthalpy Based Model of Cavitation. *ASME Journal of Fluids Engineering*, 226, pp. 63 - 70.

Baum, H. 2001. *Einsatzpotentiale Neuronaler Netze bei der CAE-Tool unterstützten Projektierung fluidtechnischer Antriebe*. Dissertation RWTH Aachen University, Shaker Verlag, Aachen, ISBN 3-8265-9659-5.

Beater, P. 1999. *Entwurf hydraulischer Maschinen*. VDI-Buch, Springer, Berlin

Bohn, D. 2008. *Ähnlichkeitsprobleme des Maschinenbaus*. Vorlesungsumdruck, IDG RWTH Aachen University.

Eich, O. 1979. *Entwicklung geräuscharmer Ventile der Ölhydraulik*. Dissertation RWTH Aachen University, Verlag Mainz.

Idelchik, I. E. 2007. *Handbook of hydraulic resistances*. 4th revised and augmented edition, Begell House, Inc., New York, ISBN: 978-1-56700-251-5.

Jungemann, M. 2005. *1D Modellierung und Simulation des Durchflussverhaltens von Hydraulikkomponenten bei sehr hohen Drücken unter Beachtung der thermodynamischen Zustandsgrößen von Mineralöl.* Düsseldorf, p. 43.

Kajaste, J., Kauranne, H., Ellman, A. and **Pietola, M.** 2006. Computational Models for Effective Bulk Modulus of Hydraulic Fluid. *The 2nd International Conference on Computational Methods in Fluid Power FPNI*. Aalborg, Denmark, 7 p.

Kleppmann, W. 2008. *Taschenbuch Versuchsplanung.* 5th edition, Hanser Verlag, Munich.

Latour, C. 1996. *Strömungskraftkompensation in hydraulischen Sitzventilen.* Dissertation RWTH Aachen University.

Li, M., **Mulemane, A.**, **Lai, M. C.** and **Poola, R.** 2005. *Simulating Diesel Injectors Based on Different Cavitation Modeling Approaches*. ASME Paper No. ICES2005-1030.

Lichtarowicz, A., **Duggins, R. K.** and **Markland, E.** 1965. Discharge Coefficients for Incompressible Non-Cavitating Flow Through Long Orifices. *Journal of Mechanical Engineering Science 1959-1982*. Professional Engineering Publishing.

Luhmer, H. 1981. *Aufbau hydraulischer Netzwerke mit differenzierendem Verhalten und ihr Einsatz zur Dämpfung hydrostatischer Antriebe*. Dissertation, RWTH Aachen University.

Maré, J. - C. and **Attar, B.** 2008. Enhanced model of four way valves characteristics and its validation at low temperature. *International Journal of Fluid Power.* Vol.9, No. 3 pp. 35 - 4.

Merrit, H. E. 1967. *Hydraulic Control Systems*. John Wiley & Sons, New York.

Murrenhoff, H. 2007. *Grundlagen der Fluidtechnik – Teil1: Hydraulik*. Shaker Verlag, ISBN 3-8265-9446-0.

N.N. 2004. *Durchflussmessung von Fluiden mit Drosselgeräten in voll durchströmten Leitungen mit Kreisquerschnitt - Teil 2: Blenden*. German edition EN ISO 5167-2.

Nykänen, T., **Esqué, S.** and **Ellman, A.** 2000. Comparison of different fluid models. *Bath Workshop on Power Transmission and Motion Control PTMC*. University of Bath, UK, pp. 151 - 165.

Riedel, C., **Murrenhoff, H.** and **Stammen, C.** 2010. Physically Correct Hydraulic System Simulation with Mass Conservative Approach. *7th International Fluid Power Conference (IFK).* Aachen, Germany, Vol.1, pp. 523 - 534.

Riedel, C., **Stammen, C.** and **Murrenhoff, H.** 2009. Fundamentals of Mass Conservative System Simulation in Fluid Power. *ASME Dynamic Systems and Control Conference (DSCC).* Hollywood, CA, 12-14 September.

Riedel, H. - P. 1973. *Untersuchungen von Kavitationserscheinungen an hydraulischen Widerständen*. Dissertation RWTH Aachen University.

Roach, P. J. 1997. Quantification of Uncertainty in Computational Fluid Dynamics. *Annual Reviews of Fluid Mechanics,* Vol. 29, Palo Alto, CA, USA

Schmitt, T. 1966. *Untersuchung zur stationären und instationären Strömung durch Drosselquerschnitte in Kraftstoffeinspritzsystemen von Dieselmotoren*, Dissertation, Technical University Munich, Forschungsberichte Verbrennungskraftmaschinen Nr. 58.

Schröder, W. 2004. *Fluidmechanik*. Aachener Beiträge zur Strömungsmechanik, 7th edition, Wissenschaftsverlag Mainz, Aachen.

Singhal, A. K., **Athavale, M. M.**, **Li, H.** and **Jiang, Y.** 2002. Mathematical Basis and Validation of the Full Cavitation Model. *ASME J. Fluids Eng.,* 124, pp. 617 - 624.

Truckenbrodt, E. 1996. *Fluidmechanik*. Band 1, 4. Auflage, Springer, Berlin.

Watton, J. 2007. *Modelling, Monitoring and Diagnostic Techniques for Fluid Power Systems*. Springer-Verlag, London, 2007 ISBN 978-1-84628-373-4.

Will, D. 1986. *Einfluß der Öltemperatur auf das Durchflußverhalten von Drosselventilen*. Dissertation TU Dresden

Winklhofer, E., **Kull, E.**, **Kelz, E.** and **Morozov, A.** 2001. Comprehensive Hydraulic and Flow Field Documentation in Model Throttle Experiments Under Cavitation Conditions. *Proceedings of ILASS-Europe Conference, Zürich.*

Witt, K. 1974. *Druckflüssigkeiten und thermodynamisches Messen.* Ingenieur Digest Verlag, Frankfurt am Main.

Yang, H.Q., **Singhal, A. K.** and **Megahed, M.** 2005. *Industrial two-phase flow CFD – The full cavitation model*. von Kármán Institute for Fluid Dynamics, Lecture Series, May 23 - 27**.**

Christian von Grabe
Dipl.-Ing. Christian von Grabe studied Mechanical Engineering at RWTH Aachen University. Since 2010 he is a member of the scientific staff at the Institute for Fluid Power Drives & Controls (IFAS) at RWTH Aachen University.

Christian Riedel
Dipl.-Ing. Dipl.-Wirt.-Ing. Christian Riedel is project manager at GHH Fahrzeuge in Gelsenkirchen since 2011. Between 2007 and 2011 he was a member of the scientific staff at the Institute for Fluid Power Drives & Controls (IFAS) at RWTH Aachen University. He studied Mechanical Engineering at RWTH Aachen University and Tsinghua University, Beijing..

Christian Stammen
PD Dr.-Ing. Christian Stammen is director of Research & Development at Fluitroncs GmbH, Krefeld. From 2001 till 2008 he worked at the Institute for Fluid Power Drives & Controls (IFAS) at RWTH Aachen University after his studies in mechanical engineering and earned his Doctorate (2005) and State Doctorate degree (2009) there.

Hubertus Murrenhoff
Univ.-Prof. Dr.-Ing. Hubertus Murrenhoff is director of the Institute for Fluid Power Drives & Controls (IFAS) at RWTH Aachen University. Main research interests cover hydraulics and pneumatics including components, systems, controls, simulation programs and the applications of fluid power in mobile and stationary equipment.